JOURNAL OF QUATERNARY SCIENCE (2024) **39**(2) 277–288 ISSN 0267-8179. DOI: 10.1002/jqs.3584

JQS Journal of Quaternary Science QRA Quaternary Research Association

Rapid deglaciation of the La Vega gorge (Sierra de Gredos, Iberian Peninsula) at the end of the global Last Glacial Maximum

JESÚS ALCALÁ-REYGOSA,[1]* NÉSTOR CAMPOS,[2] IRENE SCHIMMELPFENNIG,[3] JORGE SANJURJO-SÁNCHEZ,[4] LAETITIA LÉANNI,[3] JOSÉ JUAN ZAMORANO[5] and ASTER TEAM[3†]

[1]Departamento de Geografía, Facultad de Filosofía y Letras, Universidad Autónoma de Madrid, Calle Francisco Tomas y Valiente, 1, Campus de Cantoblanco, Madrid, 28049, España
[2]Department of Geology, Geography and Environment, University of Alcalá, C/Colegios 2, Alcalá de Henares, 28801, Spain
[3]Aix Marseille Univ, CNRS, IRD, INRAE, Coll France, CEREGE, Aix-en-Provence, France
[4]Instituto Universitario de Xeoloxía, Universidade da Coruña. ESCI, Campus de Elviña, A Coruña, 15071, Spain
[5]Instituto de Geografía, Universidad Nacional Autónoma de México, Ciudad Universitaria, Ciudad de México, 04510, Mexico

Received 11 November 2022; Revised 16 November 2023; Accepted 27 November 2023

ABSTRACT: Previous studies from the Iberian Central System and other mountains of the Iberian Peninsula and Europe suggest that deglaciation in this area occurred at the end or immediately after the global Last Glacial Maximum (LGM, 26.5–19 ka). In this research, we investigate the timing and speed of deglaciation of the palaeoglacier in La Vega gorge (Iberian Central system) since the global LGM, dating the outer moraines, glacially polished bedrock and glaciofluvial deposits by means of *in situ* cosmogenic ^{10}Be and optically stimulated luminescence. The results show that one intermediate arc located at the outer frontal moraine system has an age of ~21 ka, being consistent with the global LGM. Deglaciation began at ~21–19 ka, speeding up at ~19 ka. We estimate that around 4–5 km of the palaeoglacier receded in ~1–2 kyrs since ~19 ka, leaving La Vega gorge probably ice-free at ~18 ka. Therefore, our data confirm that deglaciation in Sierra de Gredos began at the end of the global LGM, characterised by a rapid and massive retreat of glaciers.

KEYWORDS: ^{10}Be cosmic ray exposure; deglaciation; global Last Glacial Maximum; optically stimulated luminescence

Introduction

The highest mountains of the Iberian Peninsula have been intensely affected by Quaternary glaciations. One of the coldest events of the Quaternary is the global Last Glacial Maximum (LGM), which occurred between 26.5 and 20.0/19.0 ka (Clark et al., 2009), when the Earth's glaciers reached their last maximum volume. However, the ages from the glacial record of many mountains of the Iberian Peninsula, obtained with different methods, such as cosmic ray exposure (CRE) and optically stimulated luminescence (OSL), suggest that the maximum extent of the glaciers took place thousands of years before the global LGM in the Pyrenees, the Cantabrian Mountains and Sierra Nevada or almost coincided with the global LGM in the Iberian System (Oliva et al., 2019).

In the Iberian Central System, which includes Sierra de Gredos, peripheral deposits (alignments of large glacial boulders) are slightly older (3 kyr) than the global LGM (Domínguez-Villar et al., 2013), whereas large main moraine ages are in agreement with the global LGM in Peñalara peak (Palacios et al., 2012a; Domínguez-Villar et al., 2013), the Los Pelados-El Nevero Massif (Carrasco et al., 2016), the Gredos gorge (Sierra de Gredos; Palacios, de Marcos, Vázquez-Selem 2011), the Pinar valley (Sierra de Gredos; Palacios et al., 2012b), the La Vega gorge (Sierra de Gredos; Domínguez-Villar et al., 2013), the Sierra valley (Sierra de Gredos; Domínguez-Villar et al., 2013), Los Caballeros valley (Sierra de Gredos; Domínguez-Villar et al., 2013), and the upper basin of the Cuerpo de Hombre River (Sierra de Gredos; Domínguez-Villar et al., 2013; Carrasco et al., 2015).

Nevertheless, available data on the deglaciation pattern suggest a rapid glacier retreat at the end or just after the global LGM in the French and Spanish Pyrenees (Calvet et al., 2011; Palacios et al., 2015; Delmas, 2015), the Gredos gorge (Sierra de Gredos; Palacios, de Marcos, Vázquez-Selem 2011) and Sierra Nevada (Palacios et al., 2016), and less marked in Peñalara peak (Palacios et al., 2012a). Other Iberian mountains where the recession of ice masses at the end of the LGM has been documented are Cuerpo de Hombre River (Sierra de Gredos; Carrasco et al., 2015) and the Cantabrian mountains (Rodríguez-Rodríguez et al., 2018). European mountain-glacier and ice-sheet recession at the end or immediately after the global LGM has also been reported elsewhere, such as in the Kavron valley (Turkey; Akçar et al., 2007), the Tatra mountains (Poland; Makos et al., 2013), the Greenland, Scandinavian and British–Irish ice sheets (Clark et al., 2009; Vasskog et al., 2015) and especially in the Alps, where most of the ice disappeared in a short time (~1–2 kyrs) such as the Rhine valley (80% of ice mass was lost at 18 ka) (Ivy-Ochs et al., 2004, 2008, Ivy-Ochs, 2015; Reitner, 2007; Dielforder & Hetzel, 2014; Reber et al., 2014; Wirsig et al., 2016).

In this study, a new chronological setting of the glacial record from La Vega gorge, located in the Sierra de Gredos (Central System, Iberian Peninsula; Figure 1), is presented. We test whether the formation of the main moraines from La Vega gorge is coeval with the global LGM, and if massive deglaciation occurred at the end of this event, similar to the

*Correspondence: Jesús Alcalá-Reygosa, as above.
Email: jesus.alcala@uam.es
†Consortium: ASTER Team

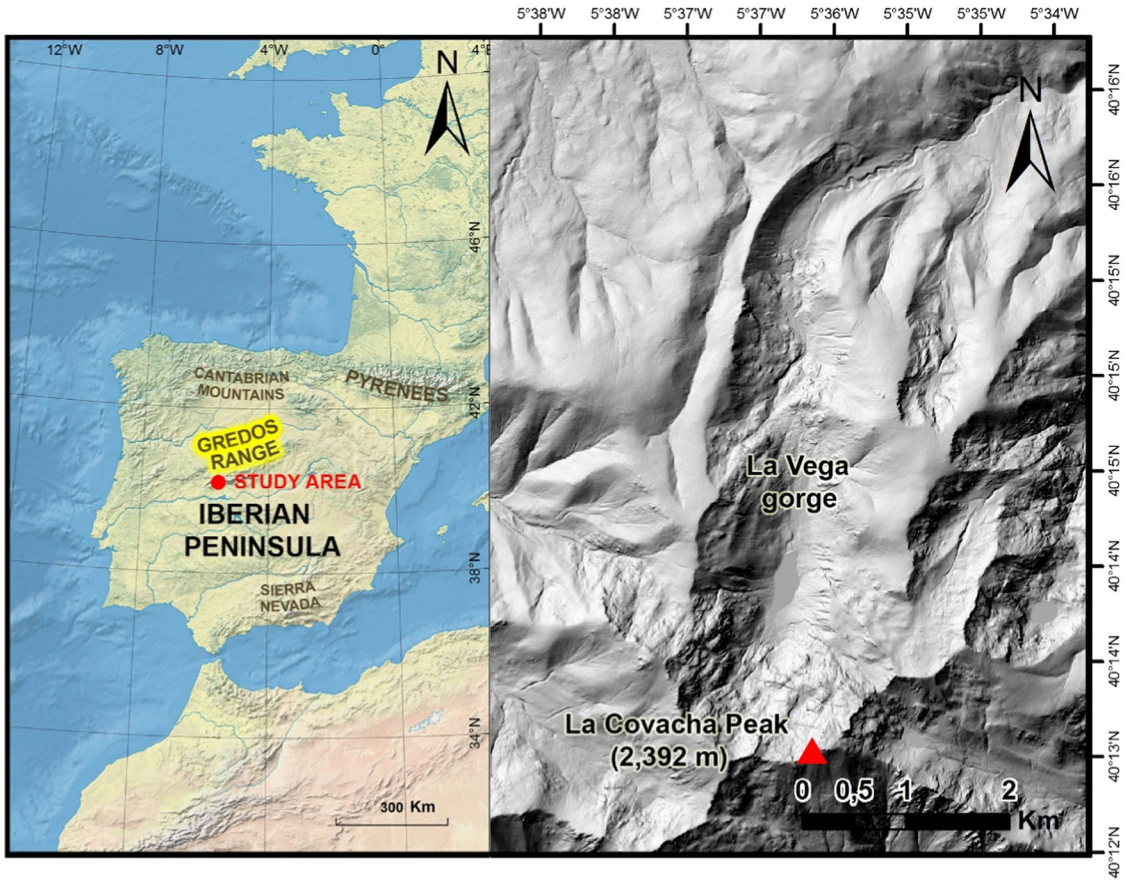

Figure 1. Location of La Vega gorge (Sierra de Gredos; Iberian Peninsula). [Color figure can be viewed at wileyonlinelibrary.com]

findings in most previous studies from the Iberian Central System and other mountains of the Iberian Peninsula and Europe. Thus, we have combined ^{10}Be CRE and OSL dating to establish a chronological record of glacial and glaciofluvial geomorphic features from La Vega gorge. As these landforms display a well-preserved sequence, La Vega gorge is particularly well suited for carrying out glacial reconstruction and deglaciation studies.

Study area

The Sierra de Gredos is located in the middle of the Central Range, a mountain system that crosses the centre of the Iberian Peninsula from northeast to southwest (40–41° N). The main alignments have a main east–west direction except some areas which follow a northeast–southwest direction. The highest peak, called Almanzor peak, reaches 2591 m asl. Around 25 km to the west of Almanzor peak appears La Covacha massif (40°13′4″ N, 5°35′51″ W; 2392 m asl) where large glacial valleys and cirques are preserved as La Vega (Figures 1 and 2).

The relief of the Sierra de Gredos is characterised by a fault block system controlled by a main normal east–west fracture network complex reactivated during the Alpine orogeny (De Vicente, 2004: Carrasco et al., 2022). The lithology of the whole Sierra de Gredos is uniform and it is composed of granodiorites (quartz-bearing) derived from intrusions during the Variscan Orogeny (Pedraza et al., 2013). This morpho-structural context conditioned the formation of the main glacial valleys of Sierra de Gredos, the spatial patterns of which follow the main fracture system directions (east–west/north–south/north-northeast–south-southwest) (Vidal-Box, 1934, 1936; Martinez de Pisón and Muñoz, 1972; Carrasco et al., 2022).

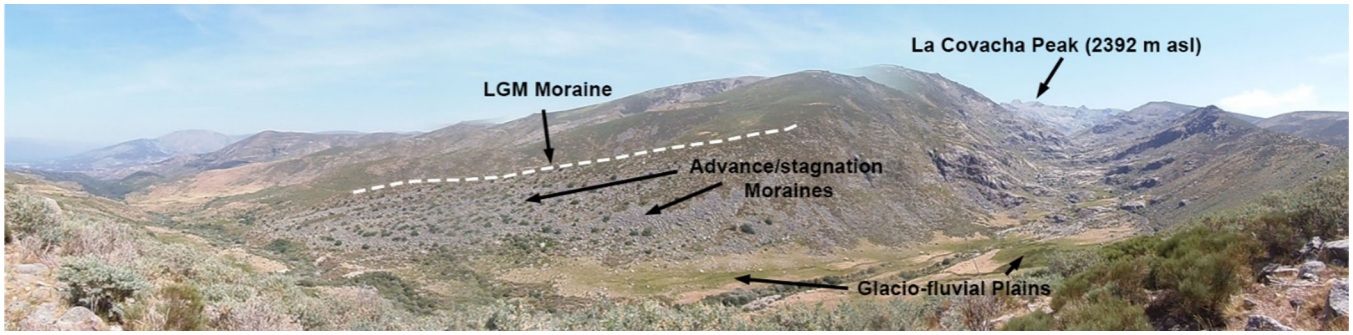

Figure 2. Panoramic view of La Vega gorge showing the glacial U-shape morphology, the moraine record and the glaciofluvial plain. View from the north. [Color figure can be viewed at wileyonlinelibrary.com]

According to Domínguez-Villar et al. (2013), the climate of the Sierra de Gredos was wet and cold between 29 and 25 ka BP, leading to the maximum local extent of glaciers, and cooler and drier between 23 and 19 ka BP. A similar palaeoclimate context has been reported for the Iberian Peninsula during the global LGM based on marine and terrestrial records (speleothem, lake sequences) (Moreno et al., 2010, 2012). However, it should be noted that there is a controversial period between 19 and 18 ka when signals of relatively warm temperatures and cold/arid conditions have been recorded (Moreno et al., 2010). Today the climate is cold and humid in winter and spring, associated with the frequent arrival of Atlantic depressions from the southwest, and dry and warm in summer due to the influence of the Azores anticyclone (Palacios et al., 2012b). On the summits (2400 m asl), the mean annual temperature is around 3°C and the annual precipitation on the north slope is 2000 mm at 2000 m asl, 77% of which falls as snow (Palacios et al. 2010). The modern 0°C isotherm is located around 2800 m asl and the snow cover remains on the ground for an average of 180–300 days per year between 2000 and 2300 m asl (Muñoz et al., 1995). Quantitative snow cover data at the altitudes of the sample sites are not available, but we estimate that in some years there could be a thin snow cover for as long as 1–2 months.

In the La Vega valley, a prominent moraine complex of impressive size (~ 2 km long and 150 m high), sharp crests and a well-preserved morphology (Campos et al., 2018) are observed (Figures 2 and 3). The frontal part of the moraine complex is composed of several successive ridges, while the lateral moraine deposits are characterised by one massive and nested crest and a few recessional sub-ridges (Figure 5). The outer moraine ridge was built during the global LGM, based on ^{10}Be dating (Domínguez-Villar et al., 2013). According to Campos et al. (2019), the palaeoglacier covered an area of 34.79 km^2 and reached a maximum ice thickness of 366 m. The ice volume was 34.25 × 10^8 m^3, and the mean equilibrium line altitude was located at 1932 m asl. A glaciofluvial plain formed by several thick deposits and enclosed by the frontal and lateral moraines is found between 1450 and 1550 m asl (Figures 2 and 3). Along its central axis, this glaciofluvial plain has been fluvially incised over a depth of around 10–15 m, forming a terrace system, which displays sharp edges due to the lateral erosion (Campos et al., 2018). Up valley, above ~1520 m asl, a large area is characterised by glacially polished bedrock reaching the summit (La Covacha) (Figure 4). Here, active geomorphological processes occur such as gelifraction, leading to rocky escarpments, debris flows and alluvial fans.

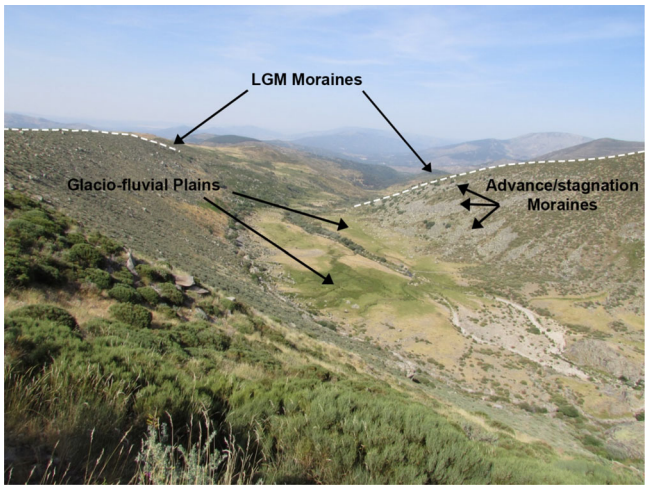

Figure 3. Photograph of the glaciofluvial and moraine deposits preserved in La Vega gorge. [Color figure can be viewed at wileyonlinelibrary.com]

Methods

Sampling strategy and treatment of the samples for ^{10}Be CRE dating

The lithology of the La Vega gorge is a compound of quartz-bearing granites, which is why we selected *in situ*-produced cosmogenic ^{10}Be dating to determine the exposure ages of the moraines, polished and striated bedrock surfaces and one glaciofluvial deposit. Ten samples were taken with a hammer and chisel from the top ~5 cm of flat-topped solid rock surfaces. Six of them were collected from >1 m high, stable boulders embedded or lying on an intermediate arc of the outer frontal moraine system (BARCO 3, 4; VEGA 5, 6; 1465 m asl), on the main crest of the massive nested left-lateral moraine (VEGA 1; 1665 m asl) and on a glaciofluvial deposit close to the frontal moraine system (BARCO 1; 1480 m asl). The other four samples were taken from polished and striated bedrock surfaces (VEGA 2, 3, 4a and 4b) located at 1560, 1550 and 1780 m asl, respectively. The distance between the four sampled boulders from the outer frontal moraine system and the upmost sampled polished and striated bedrock surface (VEGA 4) is around 4 km (Figure 5).

To minimise potential bias from post-depositional processes in the ^{10}Be surface concentrations, all the samples were collected from well-preserved surfaces without evidence of significant erosion, weathering or boulder toppling and from protruding geometries to keep to a minimum the effects of surface shielding by snow and soils (Table 1). Shielding from the surrounding topography was determined by measuring the altitudes of angular points on the horizon line with respect to the sample position, using a hand-held inclinometer, and later calculating the topographic shielding factor with the online calculator of Balco et al. (2008) (http://stoneage.ice-d.org/math/skyline/skyline_in.html) (Table 1).

The physical treatment of the samples was performed at Universidad Complutense de Madrid (Spain). Here, lichens, mosses and other organic matter were removed from the samples with a brush and then they were crushed with a roller grinder and sieved to retrieve the grain-size fraction (0.25–0.85 mm). The isolation of quartz and the chemical extraction of ^{10}Be for accelerator mass spectrometry (AMS) measurement was carried out at the Centre Européen de Recherche et d'Enseignement des Géosciences de l'Environnement (CEREGE; France).

To isolate the quartz from the bulk rock, a magnetic separator (Frantz LB-1) was used until all magnetic minerals were discarded. Then, the non-magnetic fraction experienced several chemical attacks with a mixture of concentrated hydrochloric (HCl) and hexafluorosilic (H_2SiF_6) acids to dissolve the remaining non-quartz minerals. The residual impurities were dissolved during the decontamination process of meteoric ^{10}Be by three successive partial dissolutions with concentrated hydrofluoric acid (HF).

The chemical protocol from Brown et al. (1991) and Merchel and Herpers (1999) was adapted for the subsequent beryllium extraction. About 20 g of purified quartz (Table 2) was mixed with ~100 µl of an in-house carrier solution containing 3025 µg/g of ^{9}Be and dissolved in HF. Following the same protocol as for the samples, a chemistry blank was processed. After the evaporation of the resulting solution and redissolution in a HCl acid solution, the samples experienced a series of alternating $Be(OH)_2$ precipitations in ammonia,

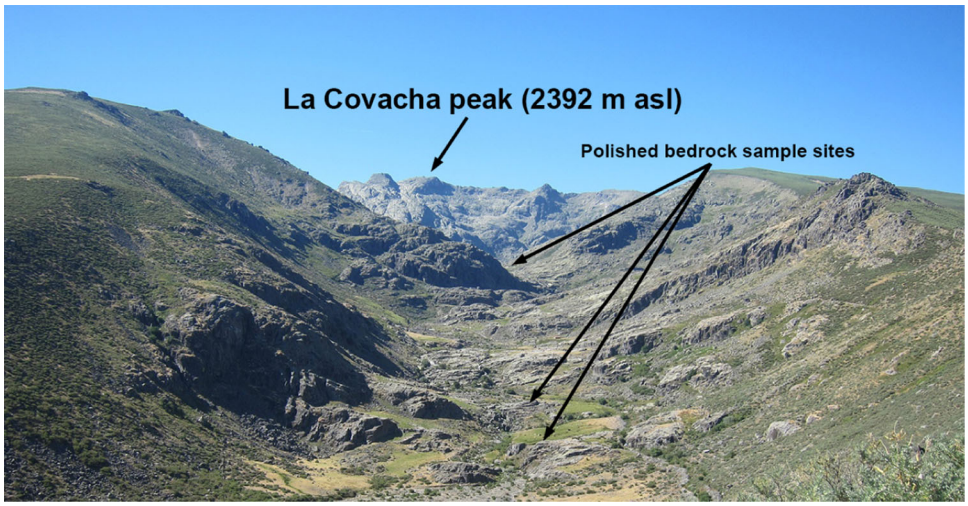

Figure 4. View, from the north, of the upper part of La Vega gorge showing the sites of the glacially polished bedrock samples. [Color figure can be viewed at wileyonlinelibrary.com]

redissolution in HCl and elution through ion exchange columns to remove iron, boron and other elements. The last $Be(OH)_2$ precipitate was oxidised to BeO at 700°C. The final BeO was mixed with niobium powder and loaded on cathodes to analyse the $^{10}Be/^{9}Be$ ratios at the French national AMS facility ASTER (CEREGE) (Arnold et al., 2010) in the year 2015, using ion source 1. The measurements at ASTER were calibrated against in-house standard STD-11, applying an assigned $^{10}Be/^{9}Be$ ratio of 1.191 (±0.013) × 10^{-11} (Braucher et al., 2015). The $^{10}Be/^{9}Be$ ratios were corrected by subtracting the measured chemistry blank $^{10}Be/^{9}Be$ ratio. A ^{10}Be half-life of 1.387 (±0.01) × 10^{6} years was used (Chmeleff et al., 2010; Korschinek et al., 2010).

We obtained the ^{10}Be CRE age with the online CREP exposure age calculator (Martin et al., 2017; http://crep.crpg.cnrs-nancy.fr), using the time-dependent 'Lm' scaling method of Lal/Stone (Lal, 1991; Stone, 2000; Nishiizumi et al., 1989; Balco et al., 2008), the ERA40 atmospheric model (Uppala et al., 2005) and the geomagnetic database by Muscheler et al. (2005) in combination with the worldwide mean ^{10}Be spallation production rate of 4.13 ± 0.20 atoms g^{-1} yr^{-1}, that was calibrated in the ICE-D production rate database linked to CREP. We considered a rock density of 2.7 g cm^{-3}.

The resulting individual ^{10}Be CRE ages are given in the text with their analytical uncertainties only for internal comparison. The internal consistency of several ages determined from the same geomorphic landform (the intermediate morainic arc and bedrock sample spot VEGA 4) was tested using the Chi^2-test of Ward and Wilson (1978) at the 2-sigma confidence level. In Table 2, the individual ages are shown with their full uncertainties (analytical and production rate uncertainties) to allow for comparison with the results from other dating techniques. Due to the short duration of the snow cover during winter, up to 1–2 months, we think that it is not necessary to perform a snow cover correction.

OSL dating

Four samples from glaciofluvial deposits were taken for OSL dating to determine the beginning of deglaciation by hammering 30 cm long and 5 cm wide steel cores into sediment profiles (Figures 6 and 7). The cores were opened under subdued red light in the Luminescence Laboratory of the University of La Coruña. The grains from the central part of the cores were dried and sieved to obtain the 180–250 µm grain-size fraction. The grains were treated with HCl and H_2O_2 to remove carbonates and organic matter, respectively. Feldspar and heavy minerals were separated using sodium polytungstate solutions of 2.62 g cm^{-3} and 2.70 g cm^{-3} specific gravity. The obtained quartz-enriched grains were etched in concentrated HF to remove any remaining feldspars and to etch the surface of the quartz grains. HCl was used to remove any remaining soluble fluorides (Viveen et al., 2014). To check whether other minerals than quartz were present in the obtained grains, infra-red (IR) stimulation was used. IRSL signals were observed for all samples except BARCO-2a. Two new density separation steps were carried out with the same result. X-Ray diffraction analyses of the three samples other than BARCO-2a showed small peaks of microcline present as inclusions. These microcline inclusions could not be removed. Thus, a double single aliquot regenerative (SAR) protocol was used to measure the IRSL and OSL signals (post-IR OSL) for these samples, as suggested by Roberts and Wintle (2001). Furthermore, a K-feldspar fraction was also obtained by using a solution of sodium polytungstate of 2.58 g cm^{-3} specific gravity, etching the obtained fraction with HF. The K-rich feldspar fraction was used for IRSL measurements (Buylaert et al., 2009).

All measurements were performed in an automated Risø DA-15 TL/OSL reader system equipped with a coupled 9235QA photomultiplier tube (PMT) and a $^{90}Sr/^{90}Y$ beta source mounted on the reader emitting a 0.120 ± 0.003 Gy s^{-1} dose. For quartz grains of the sample BARCO-2a, the blue OSL signal (470 ± 30 nm) light-emitting diodes (LEDs) were used for stimulation, and an optical Hoya U-340 filter 6 mm thick placed between the aliquots and the PMT to measure the UV range emission (340 ± 80 nm) of quartz. The SAR protocol (Murray and Wintle, 2000, 2003) was used to assess the equivalent doses (D_es). For quartz-enriched fractions emitting IRSL signals, infra-red laser diodes (830 ± 10 nm) were used before blue LEDs for stimulation. The double-SAR protocol (Roberts and Wintle, 2001, 2003) was used to obtain D_es for IRSL and post-IR OSL signals. Anomalous fading tests (Watanuki et al., 2003; Sánchez et al., 2008) were carried out on these samples. For K-feldspar grains, the post-IR IRSL-SAR (post-infrared infra-red luminescence) protocol was used to assess the D_es (Buylaert et al., 2009; Thiel et al., 2012) being first grains stimulated at 50°C and later at 290°C.

The dose rates (D_r) were estimated using low background gamma spectrometry on bulk samples, measuring the ^{238}U, ^{235}U, ^{232}Th and ^{40}K decay chain activities. The conversion factors of Guerin et al. (2011) were used to assess the internal

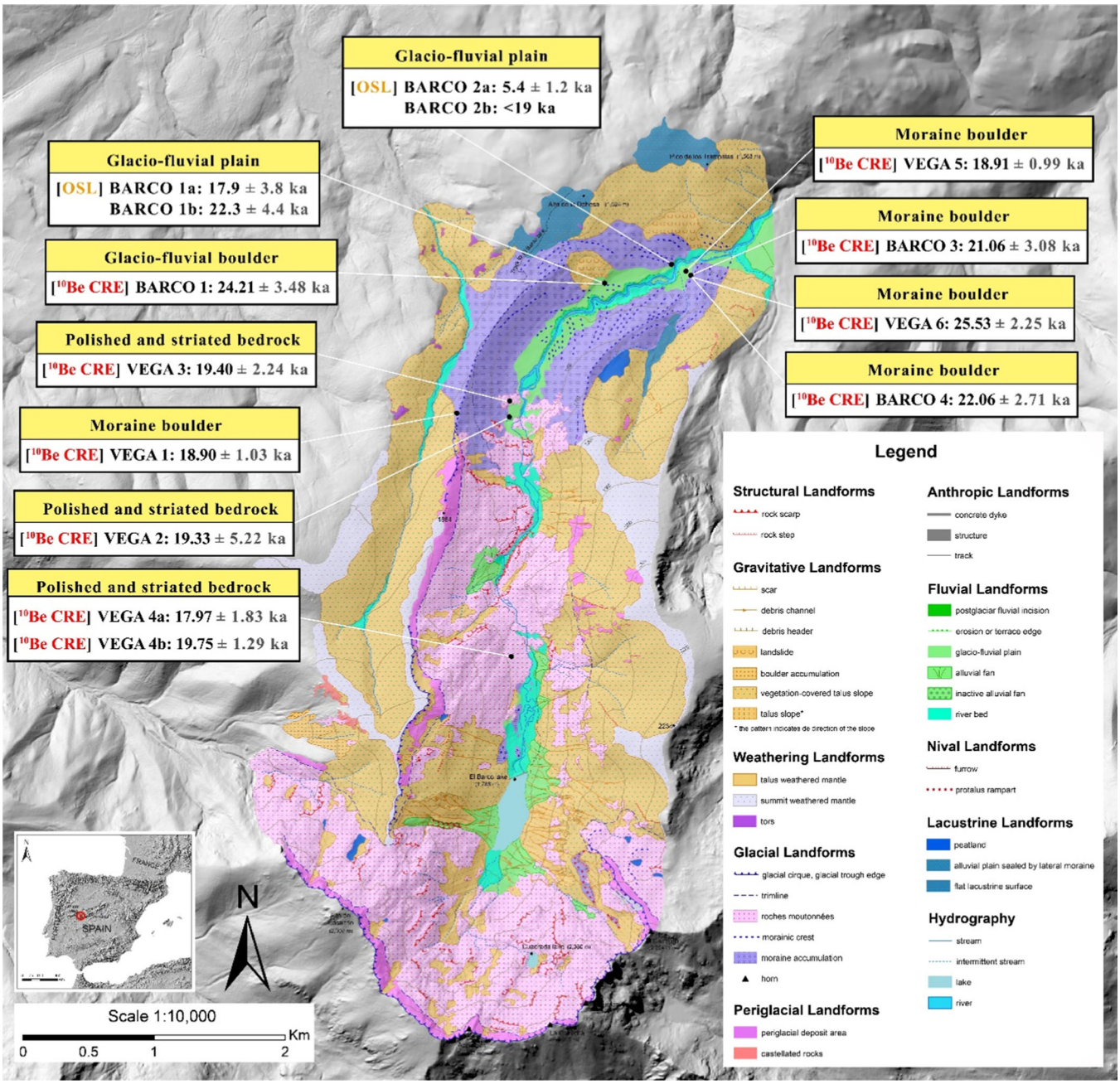

Figure 5. Location of samples on a detailed geomorphological map from La Vega gorge and the surrounding areas (modified from Campos et al., 2018). For more detailed information see Campos et al. (2018). [Color figure can be viewed at wileyonlinelibrary.com]

Table 1. Field data and sample characteristics of ^{10}Be dated samples from La Vega gorge.

Sample name	Sample type	Latitude (°N)	Longitude (°E)	Elevation (m asl)	Thickness (cm)	Shielding factor
BARCO 1	Glaciofluvial boulder	40.27	– 5.59	1476	2	0.98749
BARCO 3	Moraine boulder	40.27	– 5.59	1480	2.5	0.99575
BARCO 4	Moraine boulder	40.27	– 5.59	1448	3	0.99312
VEGA 1	Moraine boulder	40.26	– 5.61	1658	1.5	0.99354
VEGA 2	Polished and striated bedrock	40.26	– 5.60	1562	3	0.98587
VEGA 3	Polished and striated bedrock	40.26	– 5.60	1542	2.7	0.99175
VEGA 4a	Polished and striated bedrock	40.24	– 5.60	1785	1.3	0.99036
VEGA 4b	Polished and striated bedrock	40.24	– 5.60	1785	1.8	0.99036
VEGA 5	Moraine boulder	40.27	– 5.59	1453	5.0	0.99621
VEGA 6	Moraine boulder	40.27	– 5.59	1474	2.3	0.99603

Table 2. Analytical data and resulting ^{10}Be sample exposure ages calculated with the Cosmic Ray Exposure Program (CREp; Martin et al., 2017). An in-house carrier solution containing 3025 µg/g of ^{9}Be was used in the chemical treatment whereas the measurements at ASTER were calibrated against in-house standard STD-11, using a ^{10}Be/^{9}Be ratio of 1.191 (±0.013) × 10^{-11} (Braucher et al., 2015).

Sample	Sample type	Quartz (g)	AMS measured ^{10}Be/^{9}Be (10^{-13})	AMS measured error (%)	^{10}Be (at.g^{-1}) (10^{4})	Error ^{10}Be (at.g^{-1}) (10^{4})	^{10}Be CRE age (ka)	External uncertainty 1σ (ka)	Internal uncertainty 1σ without PR error
BARCO 1	Glaciofluvial boulder	20.12	2.9296E-13	13.9610	2.92E + 05	4.149E + 04	24.21	3.48	3.31
BARCO 3	Moraine boulder	21.21	2.7324E-13	14.2102	2.57E + 05	3.711E + 04	21.06	3.08	2.92
BARCO 4	Moraine boulder	20.88	2.7323E-13	11.3364	2.61E + 05	3.017E + 04	22.06	2.71	2.51
VEGA 2	Polished and striated bedrock	20.63	2.5321E-13	27.6241	2.45E + 05	6.889E + 04	19.33	5.22	5.14
Blank 1	-	-	4.5074E-15	28.0251	-	-	-	-	-
VEGA 1	Moraine boulder	20.10	2.60505E-13	3.61137	2.617E + 05	9.540E + 03	18.90	1.03	0.63
VEGA 3	Polished and striated bedrock	21.83	2.64163E-13	11.5202	2.446E + 05	2.840E + 04	19.40	2.24	2.06
VEGA 4 a	Polished and striated bedrock	20.22	2.71079E-13	10.0059	2.708E + 05	2.730E + 04	17.97	1.83	1.65
VEGA 4 b	Polished and striated bedrock	22.25	3.28756E-13	5.3005	2.991E + 05	1.596E + 04	19.75	1.29	0.96
VEGA 5	Moraine boulder	24.31	2.64114E-13	3.1825	2.193E + 05	7.042E + 03	18.91	0.99	0.55
VEGA 6	Moraine boulder	20.19	3.10127E-13	7.7540	3.101E + 05	2.421E + 04	25.53	2.25	1.91
Blank 2	-	-	2.05866E-15	20.0248	-	-	-	-	-

and external dose rates. For the pure quartz grains obtained for the sample BARCO-2a, the alpha contribution was neglected and the beta dose rate was corrected assuming that the HF etching step of quartz grains removed the surface layer of the grain (Brennan 2003). For K-feldspar grains, internal beta contributions were considered, assuming a K-content of 12.5 ± 0.5% (Huntley and Baril, 1997). Both the water content and saturation of the samples were assessed in the laboratory by weighing before and after drying, and measuring the maximum water content of the saturated samples. Cosmic dose rates were calculated according to Prescott and Hutton (1994) (Table 3).

Results

^{10}Be CRE dating

The ^{10}Be CRE ages of glacial deposits, glacially abraded bedrocks and the glaciofluvial deposit with their 1-sigma external errors, including analytical and production rate uncertainties, are shown in Figure 5 and Table 2. Table 2 also shows the 1-sigma internal (i.e. only analytical) errors of all ^{10}Be ages. The four samples from the intermediate arc of the outer frontal moraine system (1465 m asl) yield the following ages and analytical uncertainties: 25.5 ± 1.9 ka (VEGA 6), 22.1 ± 2.5 ka (BARCO 4), 21.1 ± 2.9 ka (BARCO 3) and 18.9 ± 0.6 ka (VEGA 5). We discard sample VEGA 6 as an outlier, based on the Chi-2 test. The arithmetic mean and standard deviation of the remaining three moraine ages is 20.7 ± 1.6 ka. In the upmost part of the main left-lateral moraine, we dated only one boulder (VEGA 1) and obtained an age of 18.9 ± 0.6 ka. This age is similar to the mean age of the intermediate arc although no direct stratigraphical relationship can be established with the frontal moraine system, as this lateral massive part of the moraine system might have been occupied by the glacier until shortly before its final retreat.

The four samples taken from glacially abraded bedrocks between the frontal moraine (1465 m asl) and the upper valley (1780 m asl) yield ages and analytical uncertainties of 19.4 ± 2.1 (VEGA 3), 19.3 ± 5.1 (VEGA 2), 18.0 ± 1.7 (VEGA 4a) and 19.8 ± 1.0 ka (VEGA 4b). Vega 2 has a very high uncertainty, but its nominal age is in accordance with the other bedrock ages. As both VEGA 4a and 4b were collected in the same glacially abraded bedrock, we calculate a mean age and standard deviation of 18.9 ± 1.3 ka. The ^{10}Be bedrock ages from the lower (VEGA 3) and higher (VEGA 4a and b) sample spots are younger than the mean age of the intermediate morainic arc of 20.7 ± 1.6 ka and thus stratigraphically consistent.

The ^{10}Be age obtained from the boulder BARCO 1 (24.2 ± 3.3 ka) located in the upper part of the sedimentary sequence of the glaciofluvial deposits (1480 m asl) is indistinguishable, at the 2-sigma confidence level, from the ages of the intermediate morainic arc and the bedrock spots (Figures 2, 3, 4, 5 and 8).

OSL dating

As can be observed in Table 3, the obtained ages for enriched quartz range from ~5 to ~21 ka. The enriched quartz age obtained for sample BARCO-1a is 17.9 ± 3.8 ka, and that obtained for sample BARCO-1b is 22.3 ± 4.4 ka (Table 4). The blue OSL signal of the sample BARCO-2b was above the saturation value of the growth curve. A minimum age of <19 ka was obtained for this sample from D_0 (Wintle and Murray, 2006) (Figures 5 and 7 and Table 4). A high number of aliquots (n = 66–114) were measured by both the SAR (for

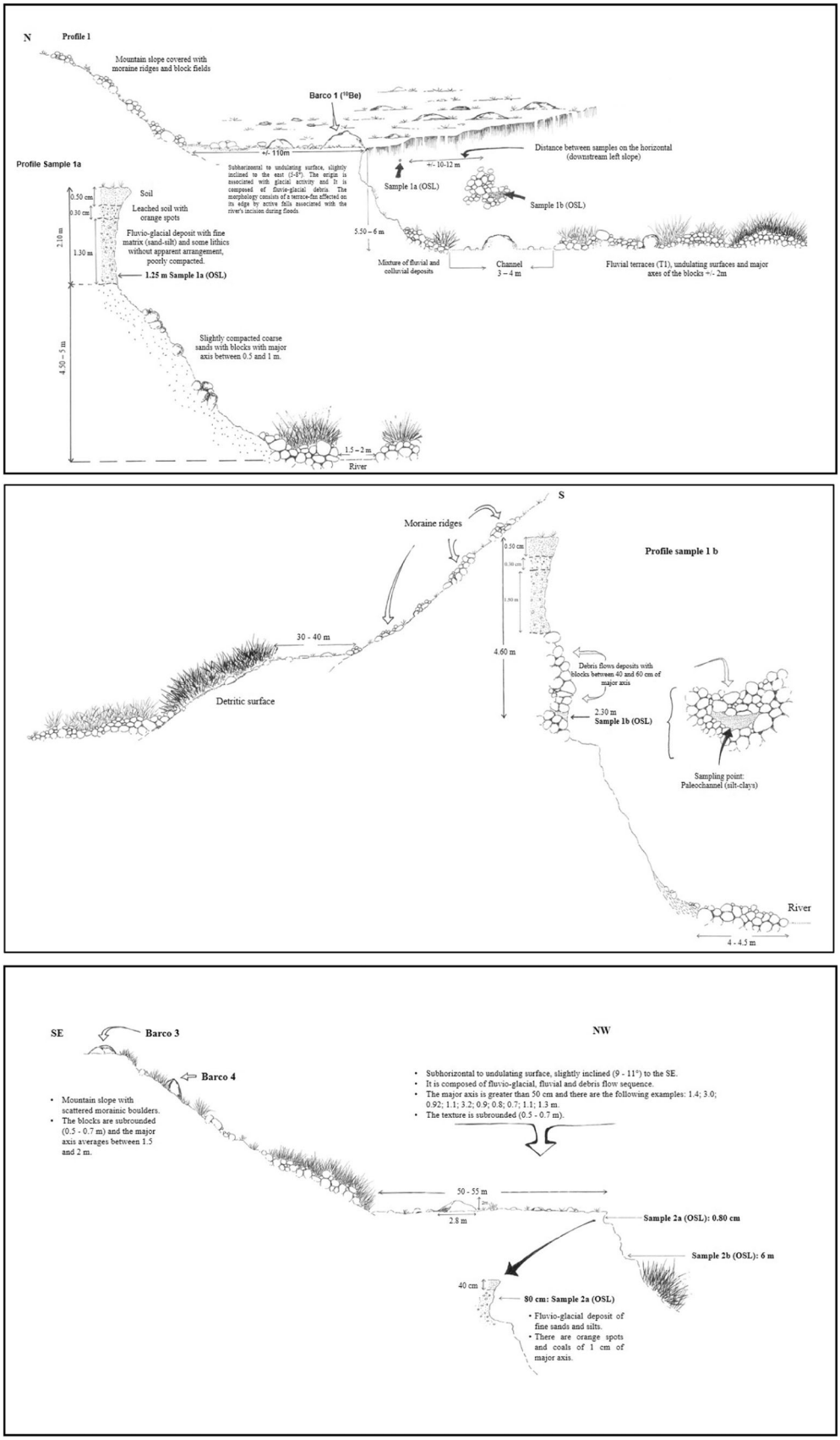

Figure 6. Detailed geomorphological context and stratigraphical columns produced during fieldwork of sampled sites in the glaciofluvial deposits and moraines of La Vega gorge for optically stimulated luminescence and ^{10}Be cosmic ray exposure dating.

sample BARCO-2a) and the double-SAR (for the other samples). About 23–30% of the aliquots were accepted, taking into account the SAR and double-SAR requirements. For the sample BARCO-2a an asymmetric distribution was observed with overdispersion of the central age of 50 ± 7%. Thus, the minimum age model was used to assess the OSL age (Galbraith et al., 1999) that resulted in an age of 5.4 ± 1.2 ka.

Both the post-IR OSL and IRSL ages from enriched quartz are coincident for the samples. However, IRSL ages obtained for K-feldspars are considerably older, as the signal was saturated

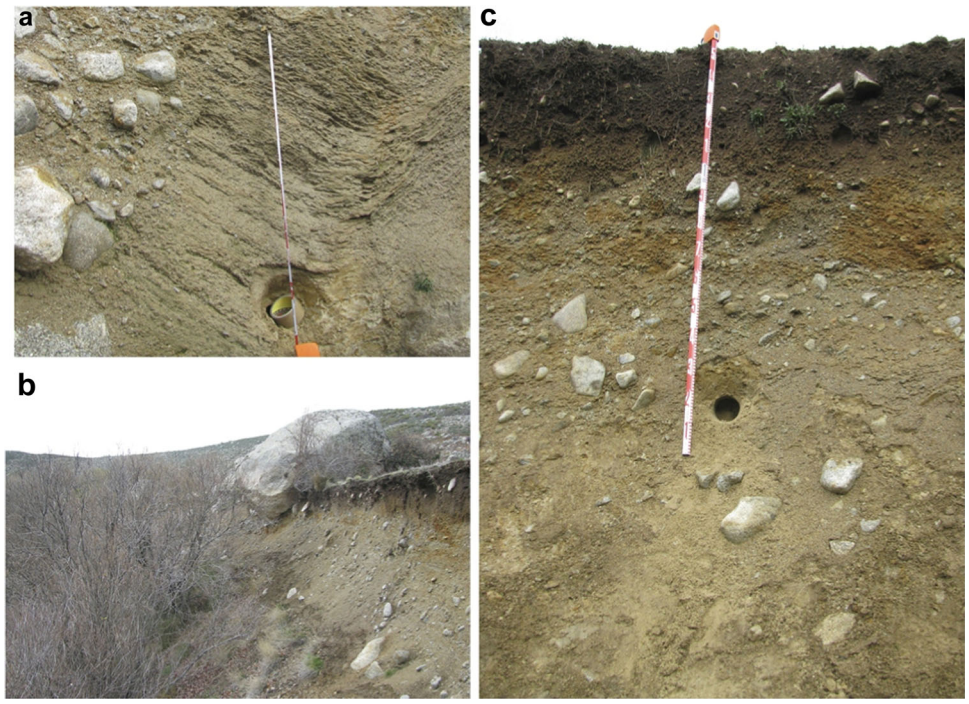

Figure 7. Detailed photographs of sampled glaciofluvial deposits for optically stimulated luminescence dating. (a) Sample 1A; (b) sample 2B and (c) Sample 1B. [Color figure can be viewed at wileyonlinelibrary.com]

Table 3. Depth of the optically stimulated luminescence samples, activity concentration of radionuclides, estimated cosmic dose rate and total dose rate.

Sample	Mineral	Depth (m)	^{40}K (Bq/kg)	^{238}U (Bq/kg)	^{226}Ra (Bq/kg)	^{235}U (Bq/kg)	^{232}Th (Bq/kg)	Cosmic dose (Gy/ka)	Dose Rate (Gy/ka)
BARCO-1a	Qz-enriched	1.25	815 ± 34	54 ± 11	61 ± 3	3.7 ± 0.3	69 ± 3	0.23 ± 0.01	4.83 ± 0.82
	K-feld								6.10 ± 0.20
BARCO-1b	Qz-enriched	1.40	885 ± 39	75 ± 15	66 ± 5	8 ± 1	64 ± 4	0.23 ± 0.01	5.10 ± 0.88
	K-feld								6.38 ± 0.29
BARCO-2a	Qz	0.8	830 ± 36	57 ± 11	50 ± 2	-	68 ± 3	0.25 ± 0.01	3.84 ± 0.29
	K-feld								5.63 ± 0.18
BARCO-2b	Qz-enriched	6	924 ± 40	58 ± 12	55 ± 2	-	53 ± 2	0.13 ± 0.01	4.20 ± 0.38
	K-feld								5.81 ± 0.23

for some of them (BARCO-1b and BARCO-2b). This is because of the effect of incomplete bleaching of the IRSL signal on K-feldspar grains, as their signal is bleached quite slowly due to daylight exposure during transport when compared with the quartz OSL signal (Duller, 2003). Indeed, Duller (2006) observed a poor bleaching of luminescence signals in glaciogenic deposits. For the post-IR ISL_{290} signals, a fading test indicated negligible anomalous fading that could affect the blue OSL signals. However, fading is observed to affect the $IRSL_{50}$ signals of the quartz-enriched grains.

The analysis of the samples provided high radionuclide activity concentrations (Table 3) that result in high dose rates, ranging from 3.84 ± 0.29 to 5.10 ± 0.88 Gy/ka for quartz grains and from 5.63 ± 0.18 to 6.38 ± 0.29 Gy/ka for K-feldspar grains. As the OSL signals were dim for pure quartz and feldspar-enriched quartz grains, multigrain aliquots of different sizes (of 1, 2, 4 and 6 mm diameter) were prepared with the 180–250 μm grain size and measured to assess the best aliquot size. It was concluded that between 5 and 20% of grains contributed to the signal and the two smallest sizes were the most suitable for dating. Bleaching tests were also performed for the $IRSL_{50}$ and post-IR OSL_{290} signals. While the blue OSL signal of the quartz of BARCO-2a was bleached up to a remaining 20% of the signal in 5 s, a slower decay was observed for the other samples. A remaining 20% of the total signal was observed after 10 s, 30 s and 60 s of stimulation for samples BARCO-2b, BARCO-1a and BARCO-1b, respectively. The dim signals are probably one of the causes of the high error obtained for the ages (~ 20%).

Discussion

The ^{10}Be CRE mean ages of the intermediate arc of the outer frontal moraine system of 20.7 ± 1.6 ka ($n = 3$) and the outer left-lateral moraine of 18.9 ± 1.0 ka, suggest that the La Vega gorge moraine system likely formed during the second half of the period of global LGM. All these ^{10}Be CRE ages match with those of the outer lateral moraine of La Vega gorge determined by Domínguez-Villar et al. (2013), at 22.5 ± 2.3 and 21.1 ± 2.8 ka, as well as most of the CRE moraine ages reported from similar settings in other valleys and mountains of the Iberian Central System (Palacios, de Marcos, Vázquez-Selem 2011; Palacios et al., 2012 a b; Domínguez-Villar et al., 2013;

Figure 8. Detailed photographs of the glacial and fluvioglacial record dated with ^{10}Be Cosmic ray exposure at La Vega gorge. (a) Glaciofluvial boulder (sample BARCO 1); (b) moraine boulder (sample VEGA 5); and (c) glacially polished bedrocks (sample VEGA 4). [Color figure can be viewed at wileyonlinelibrary.com]

Table 4. Obtained central age model D_es and minimum age model D_e for BARCO-2a*, and corrected ages after fading tests for post-IR OSL, $IRSL_{50}$ and post-IR $IRSL_{290}$ signals.

Sample	Mineral	Method	N	D_e (Gy)	Age (ka)
BARCO-1a	Enriched quartz	Post-IR OSL	27	86.6 ± 10.8	**17.9 ± 3.8**
	Enriched quartz	IRSL	42	76.8 ± 7.3	**15.9 ± 3**
	K-felds	Post-IR IRSL	13	355 ± 51	58.2 ± 8.6
	K-felds	IRSL	13	195 ± 25	-
BARCO-1b	K-felds	Post-IR OSL	26	114 ± 11	**22.3 ± 4.4**
	Enriched quartz	IRSL	23	109 ± 10	**21.5 ± 4.2**
	K-felds	Post-IR IRSL	7	<510	<80
	K-felds	IRSL	-	-	-
BARCO-2a	Quartz	OSL	36	20.7 ± 4.3*	**5.4 ± 1.2**
	K-felds	Post-IR IRSL	13	110 ± 6	19.5 ± 1.5
	K-felds	IRSL	13	65.5 ± 2.9	11.6 ± 0.6
BARCO-2b	Enriched quartz	Post-IR OSL	3	<80	**<19**
	Enriched quartz	IRSL	-	-	-
	K-felds	Post-IR IRSL	3	<530	<91
	K-felds	IRSL	-	-	-

Carrasco et al., 2015; Carrasco et al., 2016). Overall, all the reported ages support the hypothesis that the global LGM constitutes the most relevant cold climatic event during the last glaciation in the Iberian Central System. Furthermore, our chronology suggests that the climate during the first part of the LGM (26–22 ka) in the study area was cold and dry, whereas in the second part of the LGM (21–19 ka), when the moraines were formed, colder and wetter conditions would have prevailed, which are crucial for glacier expansion. This palaeoclimate scenario differs from the reconstructions derived from other geological archives, such as speleothem and lake sediments, carried out in the Iberian Peninsula (Moreno et al., 2010, 2012; Domínguez-Villar et al., 2013), which suggest cold and dry conditions between 23 and 19 ka BP. Therefore, more detailed research on the palaeoclimate characteristics of the LGM period in the Iberian Peninsula should be performed in the future.

Between 21 ka and 19 ka, an inner recessional moraine system was formed. There is a distance of around 1 km where several morainic arcs were formed between the outer intermediate moraine dated at ~21 ka and the innermost recessional moraine, which is most likely not younger than 19 ka given the moraine boulder age on the left-lateral moraine and the lowest bedrock age. This means that from its LGM maximum extent until the end of the global LGM, a glacier recession with multiple glacier stagnations took place (see Figure 5).

At 19 ka, the glacier of La Vega gorge experienced a marked and rapid retreat based on the consistent ^{10}Be CRE ages of our four glacially polished bedrock samples (~ 2 km of distance between the lowest and the highest). Thus, the 5 km long glacial valley of La Vega gorge was most likely completely ice-free by ~18 ka. In addition, one ^{10}Be CRE and three of the four OSL ages (BARCO 1a, 1b and BARCO 2b) obtained from the

deepest and intermediate thick deposits of the glaciofluvial plain support a massive retreat of the palaeoglacier of La Vega gorge at the end of the global LGM. The fourth OSL sample (2 A) collected from the upper part (1 m depth) of the glaciofluvial plain indicates two later phases of sedimentation at ~5.4 and ~3 ka, probably associated with the formation of an alluvial fan.

A rapid deglaciation of the La Vega gorge at the end of the global LGM is consistent with the data reported from other glacial valleys of Sierra de Gredos (Palacios, de Marcos, Vázquez-Selem 2011), other Iberian mountains such as the Pyrenees (Calvet et al., 2011; Palacios et al., 2015; Delmas, 2015) and Sierra Nevada (Palacios et al., 2016) and especially the European Alps (Reitner, 2007; Dielforder & Hetzel, 2014; Reber et al., 2014; Ivy-Ochs, 2015; Wirsig et al., 2016) where a similar rate of deglaciation was obtained, implying a homogeneous climate warming in the Mediterranean and central Europe at the end of the global LGM.

Other palaeoclimate records, such as speleothem from the northern Iberian Peninsula (Moreno et al., 2010), suggest both warm and cold/arid conditions between 19 and 18 ka. Our deglaciation pattern at Sierra de Gredos would confirm the warming scenario during that time. Then, together, the available glacial and speleothem records would suggest a short and intense warming period in the Mediterranean and central Europe at 19 ka before the Heinrich 1 Stadial or Oldest Dryas that took place 17.5–14.6 ka (Denton et al., 2006). Lastly, this glacier behaviour also shows the sensitive response of glaciers to changes in environmental conditions, confirming that they are key indicators of climate change now and in the future.

Although our data suggest a rapid glacier recession at the end of the global LGM at La Vega gorge, more detailed research to determine similar behaviour in other Iberian and European mountains is needed. The combination of two different dating methods (^{10}Be CRE and OSL) performed in a mountain area such as the La Vega gorge constitutes a pertinent approach to reconstruct the glacier evolution when glacial record and glaciofluvial deposits are well-preserved. Here, OSL dating of glaciofluvial deposits show ages, despite its substantial uncertainties, that are consistent with and complementary to ^{10}Be CRE dating of moraines and glacially polished bedrocks.

Conclusions

Our study is focused on the glacier evolution of the La Vega gorge located in the Iberian Central System. We combine CRE ^{10}Be and OSL to date moraine boulders, glacially polished bedrocks, glaciofluvial deposits and alluvial fans. The results suggest that the maximum glacier extent occurred at ~21 ka, suggesting a consistent synchronicity with the global LGM. Then, the glacier began to retreat at ~21–19 ka, first slowly, followed by a rapid retreat at ~19 ka. Thus, La Vega gorge was most likely ice-free by ~ 18 ka. Overall, our data confirm that the most significant glacier advance during the last glacial cycle in Sierra de Gredos occurred in the global LGM followed by a rapid and massive glacier recession which began at the end of that cold event.

Acknowledgements. This research was supported by the Mountain Warming project CGL2015-65813-R funded by the Spanish Ministry of Economy and Competitiveness, and with the help of the High Mountain Physical Geography Research Group of the Complutense University of Madrid (Spain). We would like to thank to the editor and the anonymous reviewers for their useful comments and suggestions, which improved this manuscript. The ^{10}Be measurements were performed at the ASTER AMS national facility (CEREGE, Aix-en-Provence) which is supported by the INSU/CNRS, the ANR through the 'Projets thématiques d'excellence' programme for the 'Equipements d'excellence' ASTER-CEREGE action and IRD. The first author dedicates this work with great affection to his father Felix Alcalá Pascual.

Data availability statement

The data that support the findings of this study are available from the corresponding author upon reasonable request.

Abbreviations. AMS/ASTER, french acceleratormass spectrometry; CEREGE, centre européen derecherche et d'enseignement des géosciences de l'environnement; CRE, cosmic ray exposuredating; CREP, online exposure agecalculator; ELA, equilibrium linealtitude; Des, equivalentdoses; Dr, dose-rates; HCl, hydrochloricacids; HF, hydrofluoric acid; H2SiF6, hexafluorosilicacids; IR, infra-redstimulation; LEDs, light-emitting diodes; LGM, global last glacialmaximum; OSL, optically stimulated luminescence dating; pIR IRSL-SAR, post infrared luminescence protocol; PMT, photomultiplier tube; SAR, single aliquot regenerative protocol.

References

Akçar, N., Yavuz, V., Ivy-Ochs, S., Kubik, P.W., Vardar, M. & Schlüchter, C. (2007) Paleoglacial records from Kavron Valley, NE Turkey: field and cosmogenic exposure dating evidence. *Quaternary International*, 164-165, 170–183.

Arnold, M., Merchel, S., Bourlès, D.L., Braucher, R., Benedetti, L., Finkel, R.C. et al. (2010) The French accelerator mass spectrometry facility ASTER: improved performance and developments. *Nuclear Instruments and Methods in Physics Research Section B: Beam Interactions with Materials and Atoms*, 268, 1954–1959.

Balco, G., Stone, J.O., Lifton, N.A. & Dunai, T.J. (2008) A complete and easily accessible means of calculating surface exposure ages or erosion rates from 10Be and 26Al measurements. *Quaternary Geochronology*, 3(3), 174–195.

Braucher, R., Guillou, V., Bourlès, D.L., Arnold, M., Aumaître, G., Keddadouche, K. et al. (2015) Preparation of ASTER in-house ^{10}Be/^{9}Be standard solutions. *Nuclear Instruments and Methods in Physics Research Section B: Beam Interactions with Materials and Atoms*, 361, 335–340.

Brennan, B.J. (2003) Beta doses to spherical grains. *Radiation Measurements*, 3, 299–303.

Brown, E.T., Edmond, J.M., Raisbeck, G.M., Yiou, F., Kurz, M.D. & Brook, E.J. (1991) Examination of surface exposure ages of Antarctic moraines using in-situ produced ^{10}Be and ^{26}Al. *Geochimica et Cosmochimica Acta*, 55, 2269–2283.

Buylaert, J.P., Murray, A.S., Thomsen, K.J. & Jain, M. (2009) Testing the potential of an elevated temperature IRSL signal from K-feldspar. *Radiation Measurements*, 44, 560–565.

Calvet, M., Delmas, M., Gunnell, Y., Braucher, R. & Bourles, D. (2011) Recent Advances in Research on Quaternary Glaciations in the Pyrenees. In: Ehlers, J., Gibbard, P.L. & Hughes, P.D., editors *Developments in Quaternary Science*, 15. Amsterdam, The Netherlands. pp. 127–139.

Campos, N., Palacios, D. & Tanarro, L.M. (2019) Glacier reconstruction of La Covacha Massif in Sierra de Gredos (central Spain) during the Last Glacial Maximum. *Journal of Mountain Science*, 16, 1336–1352.

Campos, N., Tanarro, L.M. & Palacios, D. (2018) Geomorphology of glaciated gorges in a granitic massif (Gredos range, Central Spain). *Journal of Maps*, 14(2), 321–329. Available at: https://doi.org/10.1080/17445647.2018.1468829

Carrasco, R.M., Pedraza, J., Domínguez-Villar, D., Willenbring, J.K. & Villa, J. (2015) Sequence and chronology of the Cuerpo de Hombre paleoglacier (Iberian Central System) during the last glacial cycle. *Quaternary Science Reviews*, 129, 163–177.

Carrasco, R.M., Pedraza, J. & Palacios, D. (2022) The glaciers of the Sierra de Gredos, *Book Iberia Land of Glaciers*. Amsterdam, Netherlands: Elservier. pp. 457–483.

Carrasco, R.M., de Pedraza, J., Willenbring, J.K., Karampaglidis, T., Soteres, R.L. & Martín-Duque, J.F. (2016) Morfología glaciar del Macizo de Los Pelados-El Nevero (Parque Nacional de la Sierra de Guadarrama). Nueva interpretación y cronología. *Bol. R. Soc. Esp. Hist. Nat. Sec. Geol*, 110, 49–66.

Chmeleff, J., von Blanckenburg, F., Kossert, K. & Jakob, D. (2010) Determination of the ^{10}Be half-life by multicollector ICP-MS and liquid scintillation counting. *Nuclear Instruments and Methods in Physics Research Section B: Beam Interactions with Materials and Atoms*, 268(2), 192–199.

Clark, P.U., Dyke, A.S., Shakun, J.D., Carlson, A.E., Clark, J., Wohlfarth, B. et al. (2009) The last glacial maximum. *Science*, 325, 710–714.

Delmas, M. (2015) The last maximum ice extent and subsequent deglaciation of the Pyrenees: an overview of recent research. *Cuadernos de Investigación Geográfica*, 41, 359–387.

Denton, G.H., Broecker, W.S. & Alley, R.B. (2006) The mystery interval 17.5 to 14.5 kyrs ago. *PAGES News*, 14, 14–16. Available at: https://doi.org/10.22498/pages.14.2.14

Dielforder, A. & Hetzel, R. (2014) The deglaciation history of the Simplon region (southern Swiss Alps) constrained by ^{10}Be exposure dating of ice-molded bedrock surfaces. *Quaternary Science Reviews*, 84, 26–38.

Domínguez-Villar, D., Carrasco, R.M., Pedraza, J., Cheng, H., Edwards, R.L. & Willenbring, J.K. (2013) Early maximum extent of paleoglaciers from Mediterranean mountains during the last glaciation. *Scientific Reports*, 3, 2034.

Duller, G.A.T. (2003) Distinguishing quartz and feldspar in single grain luminescence measurements. *Radiation Measurements*, 37, 161–165.

Duller, G.A.T. (2006) Single grain optical dating of glacigenic deposits. *Quaternary Geochronology*, 1, 296–304.

Galbraith, R.F., Roberts, R.G., Laslett, G.M., Yoshida, H.Y. & Olley, H. 1999. Optical Dating of Single and Multiple Grains of Quartz from Jinmium Rock Sherlter, Northern Australia: Part 1, Archaeometry. vol. 41. pp. 339–364.

Guerin, G., Mercier, N. & Adamiec, G. (2011) Dose-rate conversion factors: update. *Ancient TL*, 29, 5–8.

Huntley, D.J. & Baril, M.R. (1997) The K content of the K-feldspars being measured in optical dating or in thermoluminescence dating. *Ancient TL*, 15, 11–13.

Korschinek, G., Bergmaier, A., Faestermann, T., Gerstmann, U.C., Knie, K., Rugel, G. et al. (2010) A new value for the half-life of 10Be by heavy-ion elastic recoil detection and liquid scintillation counting. *Nuclear Instruments and Methods in Physics Research Section B: Beam Interactions with Materials and Atoms*, 268(2), 187–191.

Lal, D. (1991) Cosmic ray labeling of erosion surfaces: in situ nuclide production rates and erosion models. *Earth and Planetary Science Letters*, 104, 424–439.

Ivy-Ochs, S., Schäfer, J., Kubik, P.W., Synal, H.-A. & Schlüchter, C. (2004) Timing of deglaciation on the northern Alpine foreland (Switzerland). *Eclogae Geologicae Helvetiae*, 97, 47–55.

Ivy-Ochs, S., Kerschner, H., Reuther, A., Preusser, F., Heine, K., Maisch, M., Kubik, P.W. & Schlüchter, C. (2008) Chronology of the last glacial cycle in the European Alps. *Journal of Quaternary Science*, 23, 559–573.

Ivy-Ochs, S. (2015) Glacier variations in the European Alps at the end of the last glaciation. *Cuadernos de Investigación Geográfica*, 41(2), 295–315.

Makos, M., Nitychoruk, J. & Zreda, M. (2013) Deglaciation chronology and paleoclimate of the Pięciu Stawów Polskich/Roztoki Valley, high Tatra Mountains, Western Carpathians, since the Last Glacial Maximum, inferred from 36Cl exposure dating and glacier–climate modelling. *Quaternary International*, 293, 63–78.

Martin, L.C.P., Blard, P.-H., Balco, G., Lavé, J., Delunel, R., Lifton, N. et al. (2017) The CREp program and the ICE-D production rate calibration database: a fully parameterizable and updated online tool to compute cosmic-ray exposure ages. *Quaternary Geochronology*, 38, 25–49.

Martínez de Pisón, E. & Muñoz, J. (1972) Observaciones sobre la morfología del Alto Gredos. *Estudios Geográficos*, 129, 3–103.

Merchel, S. & Herpers, U. (1999) An update on radiochemical separation techniques for the determination of longlived radionuclides via Accelerator Mass Spectrometry. *ract*, 84, 215–220.

Moreno, A., González-Sampériz, P., Morellón, M., Valero-Garcés, B.L. & Fletcher, W.J. (2012) Northern Iberian abrupt climate change dynamics during the last glacial cycle: A view from lacustrine sediments. *Quaternary Science Reviews*, 36, 139–153.

Moreno, A., Stoll, H., Jiménez-Sánchez, M., Cacho, I., Valero-Garcés, B., Ito, E. et al. (2010) A speleothem record of glacial (25-11.6 kyr BP) rapid climatic changes from northern Iberian Peninsula. *Global and Planetary Change*, 71, 218–231.

Muñoz, J., Palacios, D. & De Marcos, J. (1995) The influence of the geomorphologic heritage on present slope dynamics. *Pirineos*, 145-146, 35–63.

Murray, A.S. & Wintle, A.G. (2000) Luminescence dating of quartz using an improved single-aliquot regenerative-dose protocol. *Radiation Measurements*, 32(1), 57–73.

Murray, A.S. & Wintle, A.G. (2003) The single aliquot regenerative dose protocol: potential for improvements in reliability. *Radiation Measurements*, 37, 377–381.

Muscheler, R., Beer, J., Kubik, P.W. & Synal, H.A. (2005) Geomagnetic field intensity during the last 60,000 years based on ^{10}Be and ^{36}Cl from the summit ice cores and ^{14}C. *Quaternary Science Reviews*, 24, 1849–1860.

Nishiizumi, K., Winterer, E.L., Kohl, C.P., Klein, J., Middleton, R., Lal, D. et al. (1989) Cosmic ray production rates of ^{10}Be and ^{26}Al in quartz from glacially polished rocks. *Journal of Geophysical Research: Solid Earth*, 94, 17907–17915.

Oliva, M., Palacios, D., Fernández-Fernández, J.M., Rodríguez-Rodríguez, L., García-Ruiz, J.M., Andrés, N. et al. (2019) Late Quaternary glacial phases in the Iberian Peninsula. *Earth-Science Reviews*, 192, 564–600.

Palacios, D., de Andrés, N., López-Moreno, J.I. & García-Ruiz, J.M. (2015) Late Pleistocene deglaciation in the upper Gállego Valley, Central Pyrenees. *Quaternary Research*, 83, 397–414.

Palacios, D., Andrés, N., Marcos, J. & Vázquez-Selem, L. (2012a) Glacial landforms and their paleoclimatic significance in Sierra de Guadarrama. *Central Iberian Peninsula. Geomorphology*, 139-140, 67–78.

Palacios, D., Andrés, N., Marcos, J. & Vázquez-Selem, L. (2012b) Maximum glacial advance and deglaciation of the Pinar Valley (Sierra de Gredos, Central Spain) and its significance in the Mediterranean context. *Geomorphology*, 177-178, 51–61.

Palacios, D., Gómez-Ortiz, A., Andrés, N., Salvador, F. & Oliva, M. (2016) Timing and new geomorphologic evidence of the Last Deglaciation stages in Sierra Nevada (southern Spain). *Quaternary Science Reviews*, 150, 110–129.

Palacios, D., de Marcos, J. & Vázquez-Selem, L. (2011) Last Glacial Maximum and Deglaciation of Sierra de Gredos, Central Iberian Peninsula. *Quaternary International*, 233, 16–26.

Pedraza, J., Carrasco, R.M., Domínguez-Villar, D. & Villa, J. (2013) Late Pleistocene glacial evolutionary stages in the Gredos Mountains (Iberian Central System). *Quaternary International*, 302, 88–100. Available at: https://doi.org/10.1016/j.quaint.2012.10.038

Prescott, J.R. & Hutton, J.T. (1994) Cosmic ray contributions to dose rates for luminescence and ESR dating: Large depths and long-term time variations. *Radiation Measurements*, 23, 497–500.

Reber, R., Akcar, N., Ivy-Ochs, S., Tikhomirov, D., Burkhalter, R., Zahno, C. et al. (2014) Timing of retreat of the Reuss glacier (Switzerland) at the end of the last glacial maximum. *Swiss J. Geosciences*, 107, 293–307. Available at: https://doi.org/10.1007/s00015-014-0169-5

Reitner, J. (2007) Glacial dynamics at the beginning of termination I in the eastern alps and their stratigraphic implications. *Quaternary International*, 164-165, 64–84.

Roberts, H.M. & Wintle, A.G. (2001) Equivalent dose determinations for polymineralic fine-grains using the SAR protocol: application to a Holocene sequence of the Chinese Loess Plateau. *Quaternary Science Reviews*, 20(5-9), 859–863.

Roberts, H.M. & Wintle, A.G. (2003) Luminescence sensitivity changes of polymineral fine grains during IRSL and [post-IR] OSL measurements. *Radiation Measurements*, 37(6), 661–671.

Rodríguez-Rodríguez, L., Domínguez-Cuesta, M.J., Rinterknecht, V., Jiménez-Sánchez, M., González-Lemos, S., Léanni, L. et al. (2018) Constraining the age of superimposed glacial records in mountain environments with multiple dating methods (Cantabrian Mountains, Iberian Peninsula). *Quaternary Science Reviews*, 195, 215–231.

Sánchez, J., Mosquera, D. & Montero Fenollós, J. (2008) TL and OSL dating of sediment and pottery from two Syrian archaeological sites. *GEOCHR*, 31, 21–29.

Stone, J.O. (2000) Air pressure and cosmogenic isotope production. *Journal of Geophysical Research: Solid Earth*, 105, 23753–23759.

Thiel, C., Buylaert, J.P., Murray, A.S., Elmejdoub, N. & Jedoui, Y. (2012) A comparison of TT-OSL and post-IR IRSL dating of coastal deposits on Cap Bon peninsula, northeastern Tunisia. *Quaternary Geochronology*, 10, 209–217.

Uppala, S.M., KÅllberg, P.W., Simmons, A.J., Andrae, U., Bechtold, V.D.C., Fiorino, M. et al. 2005. The ERA-40 Re-analysis. vol. 131. Quartely Journal of the Royal Meteorological Society, pp. 2961–3012. https://doi.org/10.1256/qj.04.176.

Vasskog, K., Langebroek, P.M., Andrews, J.T., Nilsen, J.E.Ø. & Nesje, A. (2015) The Greenland Ice Sheet during the last glacial cycle: Current ice loss and contribution to sea-level rise from a palaeoclimatic perspective. *Earth-Science Reviews*, 150, 45–67.

De Vicente, G. (2004). Estructura alpina del Antepaís Ibérico. [Alpine structure of Iberian "Antepaís"]. Geol España Soc Geológica España; Instituto Geológico y Minero de España Madrid.: 587–634. (in spanish).

Vidal-Box, C. (1934) Los glaciares cuaternarios de la Sierra del Bohoyo (Ávila). *Boletín Real Sociedad Española de Historia Natural*, 34, 485–486.

Viveen, W., Sanjurjo-Sánchez, J., Goy-Diz, A., Veldkamp, A. & Schoorl, J.M. (2014) Paleofloods and ancient fishing weirs in NW Iberian rivers. *Quaternary Research*, 82, 56–65.

Ward, G.K., Wilson, S.R. (1978) Procedures for comparing and combining radiocarbon age determinations: a critique. *Archaeometry*, 20, 19–31.

Watanuki, T., Murray, A.S. & Tsukamoto, S. (2003) A comparison of OSL ages derived from silt-sized quartz and polymineral grains from Chinese loess. *Quaternary Science Reviews*, 22(10-13), 991–997.

Wintle, A.G. & Murray, A.S. (2006) A review of quartz optically stimulated luminescence characteristics and their relevance in single-aliquot regeneration dating protocols. *Radiation Measurements*, 41, 369–391.

Wirsig, C., Zasadni, J., Christl, M., Akçar, N. & Ivy-Ochs, S. (2016) Dating the onset of LGM ice surface lowering in the High Alps. *Quaternary Science Reviews*, 143, 37–50.